COBEM 2023 27TH INTERNATIONAL CONGRESS OF MECHANICAL ENGINEERING

ABCM Brazilian Society of Mechanical Sciences and Engineering
27th ABCM International Congress of Mechanical Engineering
December 04-08, 2023, Florianópolis-SC, Brazil

COB-2023-1472
CHARACTERIZATION OF NANOCOMPOSITE POWDERS FOR ADDITIVE MANUFACTURING

Gustavo Scheid Prass
Federal University of Paraná, Department of Mechanical Engineering, Curitiba, PR, Brazil.
SENAI Innovation Institute in Manufacturing Systems and Laser Processing, Joinville, SC, Brazil.
gustavo.prass@ufpr.br

Victor Lira Chastinet
SENAI Innovation Institute in Manufacturing Systems and Laser Processing, Joinville, SC, Brazil.
victor.chastinet@sc.senai.br

Ana Sofia C. M. d'Oliveira
Federal University of Paraná, Department of Mechanical Engineering, Curitiba, PR, Brazil.
sofmat@ufpr.br

Abstract. *Additive manufacturing (AM) of metallic parts includes a set of techniques where three-dimensional objects are built up layer by layer using metallic powder or wire as feedstock. The use of metallic powder has its own advantages, such as the ability to blend different powders to obtain customized chemical compositions, which drives innovation in the development of new materials. In this context, nanocomposite powders can be introduced to AM processes to take advantage of their unique properties. Nanocomposite powders are materials consisting of a carrier powder, generally microparticles (MPs), and one or more types of nanoparticles (NPs) that are distributed on the MPs surface. Characterization of the nanocomposite powders is important to understand their behavior during the additive manufacturing process and to select processing parameters, leading to the production of defect-free parts with desired properties. In this study, different powder compositions were obtained by individually mixing AISI 316L with 1 wt% Cu MPs, Cu NPs, and CuO NPs. The mixtures with NPs were carried out in two steps, the first mixture was done in a mechanical mixer with pure ethanol to avoid agglomeration of the NPs and the second mixture was done in a Y-type mixer after drying (50ºC for 24 h). AISI 316L and Cu MPs both range from 75 to 150 µm as measured by dynamic image analysis (DIA). Cu NPs and CuO NPs have average particle sizes of 500 nm and 30 nm, respectively, according to the manufacturer. Scanning electron microscopy (SEM) was used to analyze powder morphology, SEM images showed that the electrolytic Cu MPs are irregular with a dendritic-like morphology and gas-atomized AISI 316L particles are mostly spherical, with satellite particles. The MPs had some porosity that was not observed in the multilayers processed by plasma transferred arc (PTA). Cu NPs and CuO NPs adhered to the surface of the carrier particles in a well-distributed manner. Energy-dispersive X-ray spectroscopy (EDS) confirmed the composition of powder mixtures. Powder flowability was evaluated using a Hall funnel with dried (80ºC for 2 h) and non-dried powder mixtures. Results showed that powder mixtures containing NPs required drying before the deposition to mitigate the negative impact of humidity on powder flowability. Deposited multilayers processed with nanocomposite powder mixtures have a similar density to those processed with atomized stainless steel, whereas powder mixtures containing Cu MPs resulted in denser multilayers.*

Keywords: *Additive Manufacturing, Nanocomposite Powder, AISI 316L, Cu, CuO.*

1. INTRODUCTION

Additive manufacturing (AM) is a technology that allows for the fabrication of complex metallic parts, in a process which involves processing the feedstock layer-by-layer (Huang et al., 2014). Among the available feedstock options, powders offer versatility in creating customized chemical compositions, enabling the development of advanced materials with tailored properties (Li et al., 2019; Dong et al., 2020; Cui et al., 2022). A particularly promising approach is the generation of nanocomposite powders, where guest nanoparticles (NPs) are incorporated into the carrier powder matrix (Zhuang et al., 2020; Soulier et al., 2022). During this process, the guest NPs adhere to the carrier particle surface, if their adhesion force surpasses their gravity force. However, this introduces changes the interaction between the carrier particles, altering critical properties, such as cohesion and flowability (Sharma and Setia, 2019).

In the context of AM, Powder Bed Fusion (PBF) and Directed Energy Deposition (DED) are two techniques where the powder characteristics plays an important role in processability. In PBF, successive thin layers of powder must be evenly spread across the powder bed to create fully dense parts (Avrampos and Vosniakos, 2022; Abu-Lebdeh et al., 2022). Similarly, in DED, a consistent powder flow through a feeding system is crucial for deposition (Mellin et al., 2017;

Garg et al., 2023). Thus, the development of advance materials for AM requires a thorough understanding of the interaction between the microparticles (MPs) and NPs, elucidating their impact on processability and the resulting properties of the fabricated parts.

As part of an ongoing project aiming to enhance the antimicrobial properties of stainless-steel by adding Cu particles to the metal matrix. This study approaches the preparation and characterization of nanocomposite powder for AM. The deposition of powder mixtures, consisting of stainless-steel powder and different Cu particles, were carried out using the plasma transferred arc (PTA) deposition process. Notably, the effect of powder characteristics on flowability and part density were assessed.

2. MATERIALS AND METHODS

Four primary materials were used to investigate the characteristics of nanocomposite powders for AM. Commonly applied in AM, gas atomized AISI 316L powder (85 – 150 µm) served as the carrier powder. As guest powder, Cu was provided in the form of Cu microparticles (Cu MP, 89 – 143 µm), Cu nanoparticles (Cu NP, about 500 nm) and CuO nanoparticles (CuO NP, about 40 nm). The stainless-steel powder was individually mixed with 1 wt% of Cu MP, Cu NP and CuO NP to obtain the powder mixtures.

For the powder mixture containing Cu MPs, the powders were dried in a furnace at 80 ºC for 2 h before being mixed in a Y-type mixer for 2 h, ensuring uniform distribution of Cu particles within the stainless-steel powder. The preparation of nanocomposite powders is more complex, as NPs tends to agglomerate in clusters, not adhering to the carrier particle surface. The dispersion of NPs was performed in an ultrasonic bath with ethanol for 300 s. The stainless-steel powder was added to the ethanol-dispersed NPs and mechanically stirred for 2 h. The ethanol was evaporated in a furnace at 50 ºC for 24 h. Finally, the dried powders were mixed in a Y-type mixer for 12 h to guarantee strong adhesion between the guest NPs and the surface of the carrier MPs.

Powder mixtures and particles morphology were assessed by optical microscopy (OM), scanning electron microscopy (SEM) and field emission gun equipped SEM (FEG-SEM). Particle size distribution, particle shape and circularity of AISI 316L powder and Cu MP were performed by dynamic image analysis (DIA) in accordance with ASTM B822-20, while their cross-section density was measured by SEM. Flow behavior of the non-dried (shelf condition) and dried (80 ºC for 2h) powder mixtures was characterized using a Hall flowmeter funnel, following ASTM B213-20.

Plasma transferred arc (PTA) was employed to deposit the powder mixtures on AISI 304L plates. Single-bead walls with 11 layers and length of 150 mm were deposited using a mass flow rate of 6 g/min, deposition speed of 100 mm/min and deposition current of 120 A (first layer) and 80 A (other layers). Argon was used as the carrier gas (0.8 L/min), plasma gas (2 L/min) and shield gas (15 L/min). The single-bead wall cross-sections were ground and polished with alumina (1 µm) to achieve a mirror-like finish. The density and chemical composition of the PTA-deposited materials were assessed by OM and X-ray fluorescence (XRF), respectively.

3. RESULTS AND DISCUSSION

XRF analysis was performed for AISI 316L powder and calculated for the powder mixtures, incorporating 1 wt% of Cu MP, 1 wt% of Cu NP and 1 wt% CuO NP. When comparing the powder mixtures, it is evident that the addition of the different Cu particles has low impact on the elemental percentage of AISI 316L. However, it should be noted that 1.0 g of CuO adds approximately 0.8 g of Cu and 0.2 g of O to the mixture. Table 1 presents the chemical composition of the powder mixtures in weight percentage.

Table 1. Chemical composition of the powder mixtures in weight percentage.

Powder mixture	Fe	Cr	Ni	Mo	Mn	S	Si	P	Cu	O	Source
AISI 316L	Bal.	17.64	12.52	3.34	1.72	0.69	0.53	0.09	-	-	XRF
AISI 316L + Cu MP	Bal.	17.47	12.40	3.31	1.70	0.69	0.52	0.09	1.00	-	calculated
AISI 316L + Cu NP	Bal.	17.47	12.40	3.31	1.70	0.69	0.52	0.09	1.00	-	calculated
AISI 316L + CuO NP	Bal.	17.47	12.40	3.31	1.70	0.69	0.52	0.09	0.80	0.20	calculated

Carbon content < 0.03 wt%

Figure 1 illustrates the OM and SEM images of the AISI 316L powder and AISI 316L + Cu MP powder mixture. Stainless-steel particles are gray (Fig. 1a) and exhibit a predominantly spherical shape with some satellite particles (Fig. 1b). At a higher magnification, the roughness of the particle surface (Fig. 1c) can be seen. The adhesive interactions between the spherical particles are greatly reduced by the surface roughness, improving powder flowability (Sharma and Setia, 2019). As a hypothesis, the surface roughness benefits the generation of nanocomposite powder, since the small wrinkles and groves serve as points of anchorage for the NPs. The Cu MPs are red-orange and are well distributed among the stainless-steel particles (Fig. 1d). In contrast, the Cu MPs are irregular in shape (Fig. 1e) and have a higher surface-to-volume ratio (Fig. 1f), which could be detrimental to the powder flowability if added in excessive quantities.

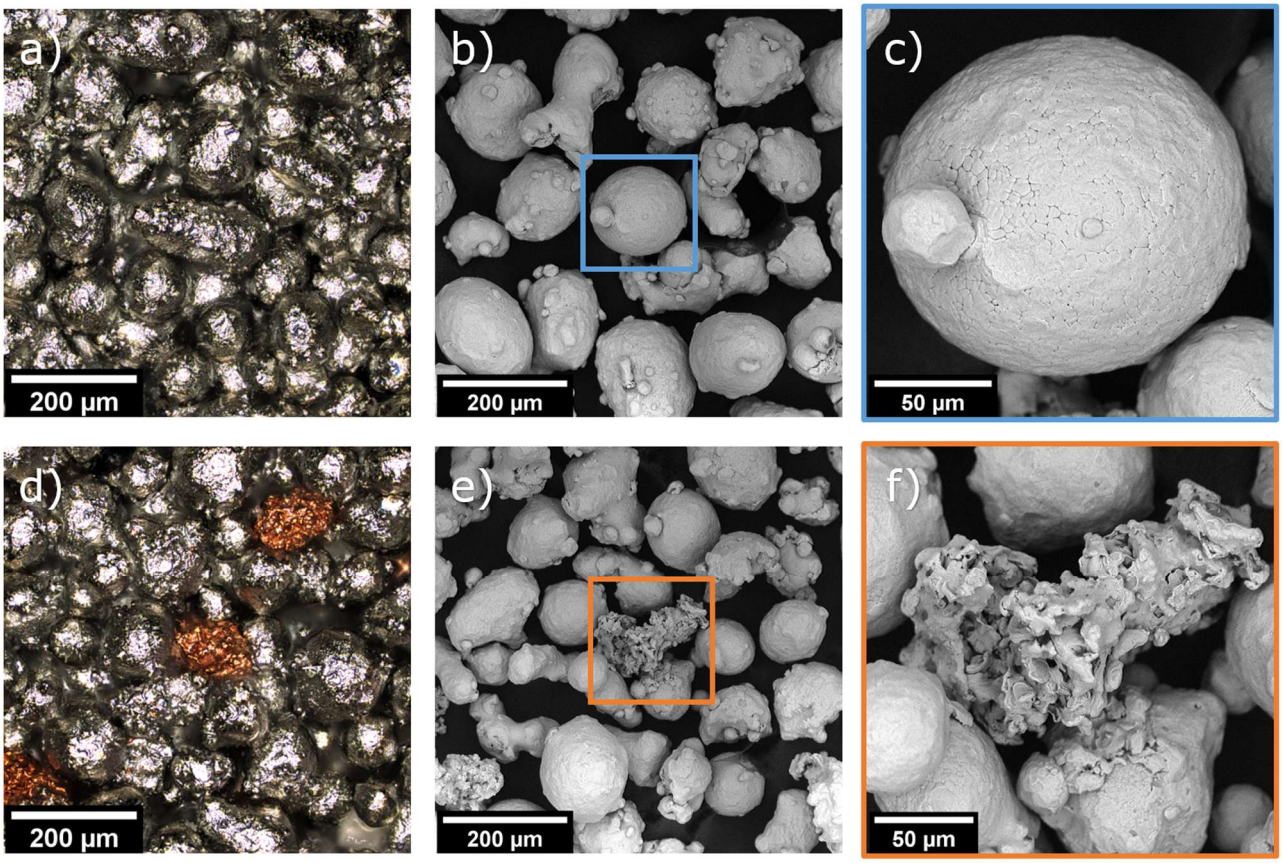

Figure 1. OM and SEM images of (a, b, c) AISI 316L powder and (d, e, f) AISI 316L + Cu MP powder mixture.

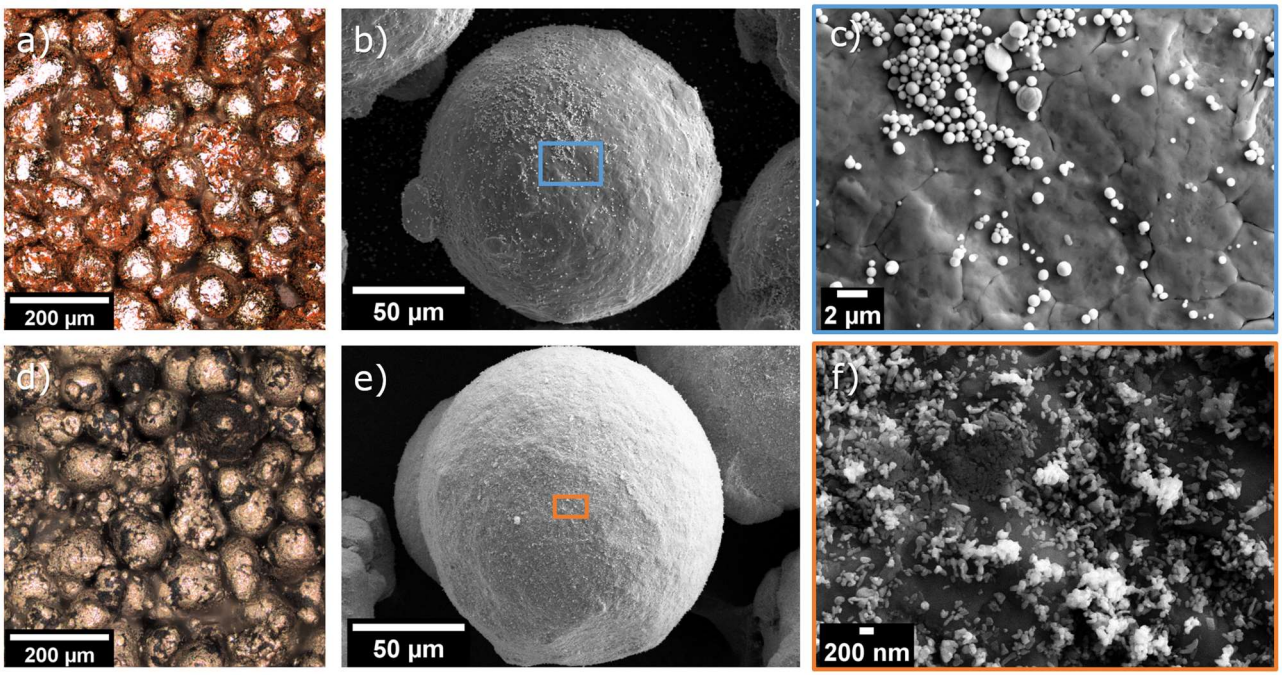

Figure 2. OM and FEG-SEM images of (a, b, c) AISI 316L + Cu NP powder mixture and (d, e, f) AISI 316L + CuO NP powder mixture.

Figure 2 presents the OM and FEG-SEM images of the nanocomposite powders of AISI 316L + Cu NP and AISI 316L + CuO NP. The carrier particles, originally gray, acquired a red-orange appearance, showcasing the presence of

guest Cu NPs (Fig. 2a). The Cu NPs are adhered to the carrier particle in a well-distributed manner, partially covering its surface (Fig. 2b). At higher magnifications, the NPs can be seen adhered to the surface individually and in clusters (Fig. 2c). The CuO NPs presence changed the color of the carrier particles to a brownish-orange color (Fig. 2d). The CuO NPs adhered to the AISI 316L particles surface (Fig. 2e). Due to its reduced size of approximately 40 nm, the NPs covered the surface almost completely (Fig. 2f).

Figure 3 provides information about powder size distribution for AISI 316L and Cu MPs, respectively. The equivalent circular area (ECA) diameter can be determined by the average size of particles in volume percentage and in number percentage. The volume distribution of AISI 316L (Fig. 3a) shows that 10% of the volume comes from particles smaller than 85.6 µm and 10% of the volume comes from particles bigger than 150.0 µm. The number distribution of AISI 316L (Fig. 3b) shows that 10% of the particles are smaller than 20.9 µm and 10% of the particles are bigger than 120.3 µm. This behavior is expected in for powders with satellite particles, since the satellites can break from the bigger particles during transportation and handling, forming new, but smaller particles. Although, due to their small size, these particles represent an insignificant volume in the powder distribution.

In comparison, the volume distribution of Cu MP (Fig. 3c) shows that 10% of the volume comes from particles smaller than 89.6 µm and 10% of the volume comes from particles bigger than 143.1 µm. This result show that the size distributions of the stainless-steel and Cu powders are in the same range, resulting in a uniform particle distribution when mixed, as seen on Fig. 1d. However, the number distribution of Cu MP (Fig. 3d) shows that 10% of the particles are smaller than 4.9 µm and 10% of the particles are bigger than 112.2 µm. The presence of a substantial number of small particles in the powder mixture could be attributed to the breakdown of irregular Cu particles. Additionally, these smaller particles may lead to disturbances in powder flowability.

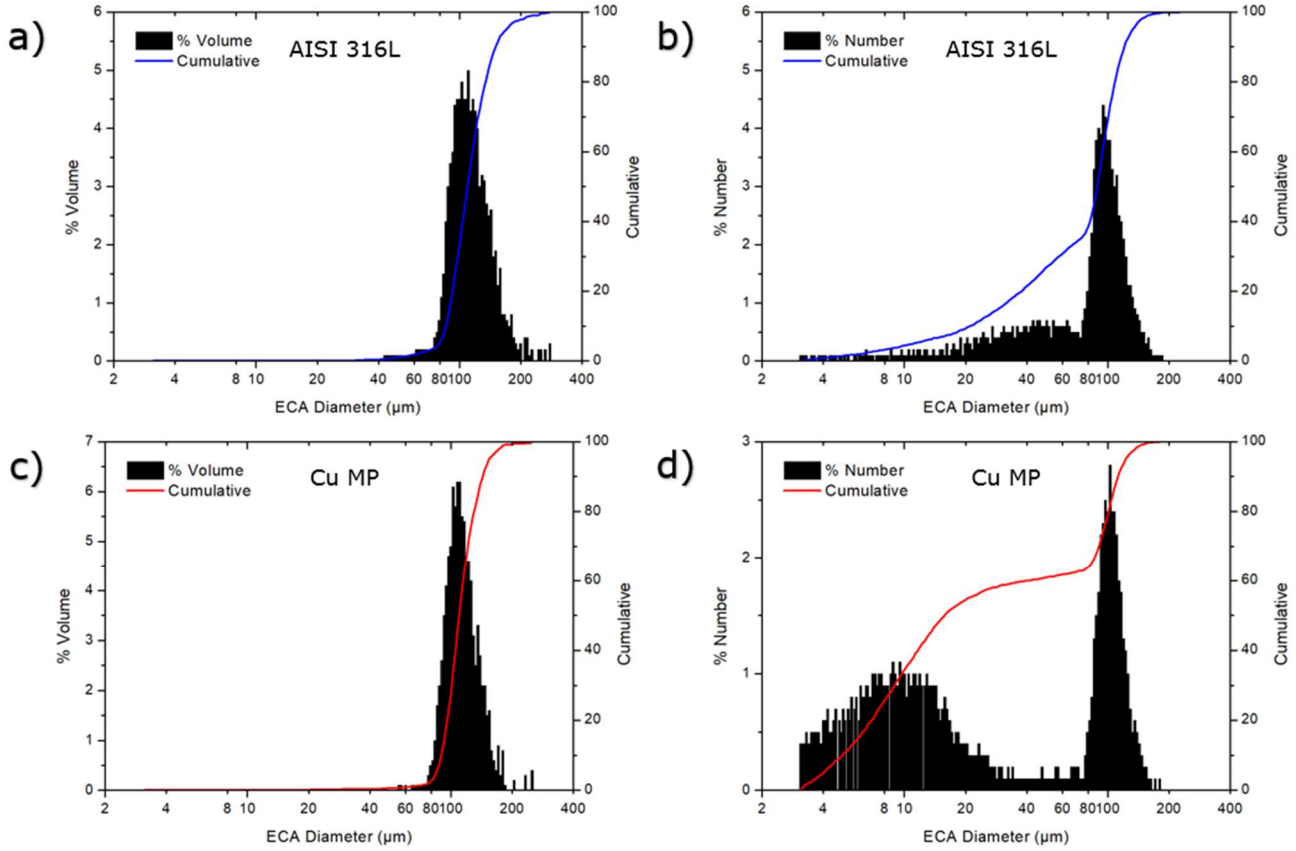

Figure 3. ECA diameter per volume and ECA diameter per number for (a, b) AISI 316L and (c, d) Cu MP.

Figure 4 offers a visual representation of AISI 316L and Cu MP particles shape and measured particle circularity by DIA. As expected, spherical stainless-steel particles are shown in sharp silhouettes (Fig. 4a), on the contrary, irregular Cu particles are represented by blurry silhouettes (Fig. 4c). The particles shape can be better described by the circularity, where a value of 1.0 represents a perfect circle. The mean circularity measured for AISI 316L and Cu MP is respectively, 0.642 ± 0.104 and 0.552 ± 0.117. This information is valuable for controlling the powder mixture for consistent powder flow in AM deposition, since higher circularity usually means better flowability.

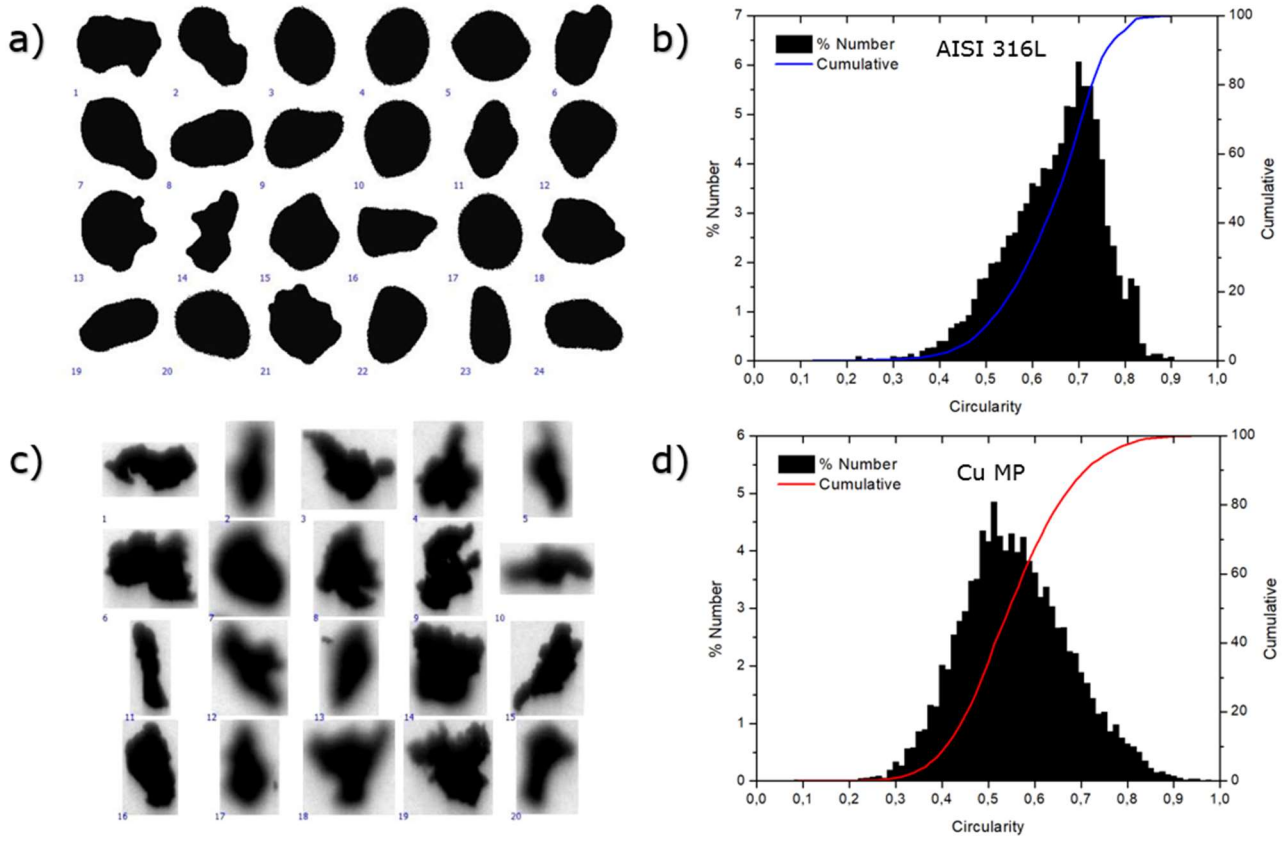

Figure 4. Particle shape and particle circularity for (a, b) AISI 316L and (c, d) Cu MP.

Hall flowmeter funnel was used to measure the flow time of the powder mixtures. Figure 5 shows the results for the non-dried (shelf condition) and dried powders (80 ºC for 2h). The lower the time for the powder to flow through the Hall funnel aperture, the better the powder flowability. The mean flow time for AISI 316L was below 35.0 s per 50 g and its flow time was not affected by a potential humidity content. Adding Cu MPs did not change the flow time, despite their irregular shape. This observation suggests that adding small amounts of irregular particles to more spherical particles can be done without hindering powder flowability.

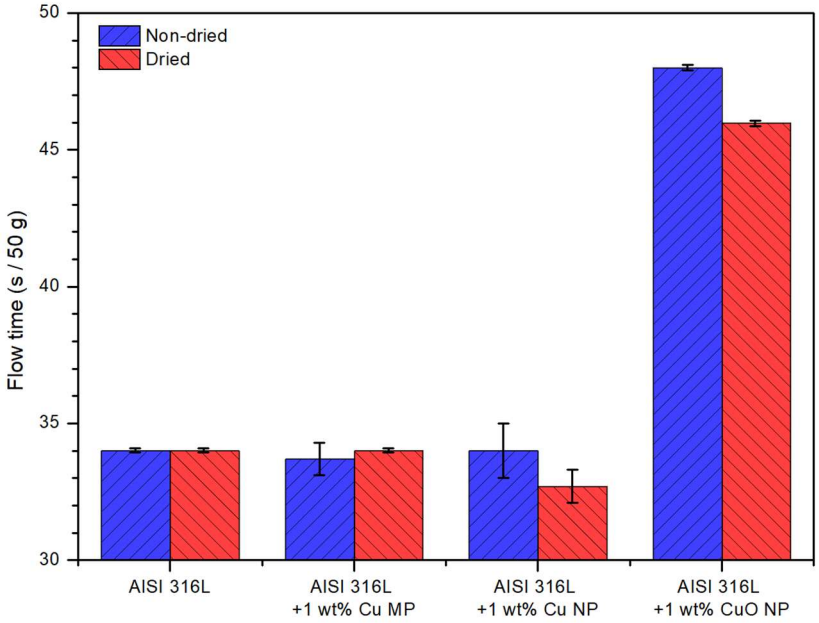

Figure 5. Hall funnel flow time for non-dried and dried powder mixtures.

The nanocomposite powder with Cu NP showed similar flow time than the stainless-steel powder in the non-dried condition and lower flow time after dried. This behavior can be explained by presence of the Cu NPs at the surface of the carrier particles, that can reduce the cohesion between the stainless-steel particles and improve flowability (Sharma and Setia, 2019). Humidity has a negative effect on the flowability of both nanocomposite powders. However, the addition of CuO NP lead to a significant increase in flow time. Due to its high surface-to-volume area, CuO NPs have high surface free energy and tends to cluster to reduce its energy, increasing the cohesion between particles and slowing down flow.

To assess the internal features of the MPs, cross-section SEM images of AISI 316L and Cu MP are shown in Figure 6. It is shown that some of the stainless-steel particles has big pores (Fig. 6a). In detail (Fig. 6b), the pores inside the particle are indicated by arrows, some pores are small (about 1 µm), but others are bigger (about 35 µm). The cross-section of the irregular Cu MPs (Fig. 6c) provides insight of the internal structures of this powder. It is possible to observe numerous voids within the particle region. The presence of pores and irregularities in the feedstock can impact the density of the parts build by AM. However, the fine tuning of processing parameters, considering the characteristics of the feedstock, should guarantee the obtention of fully dense parts.

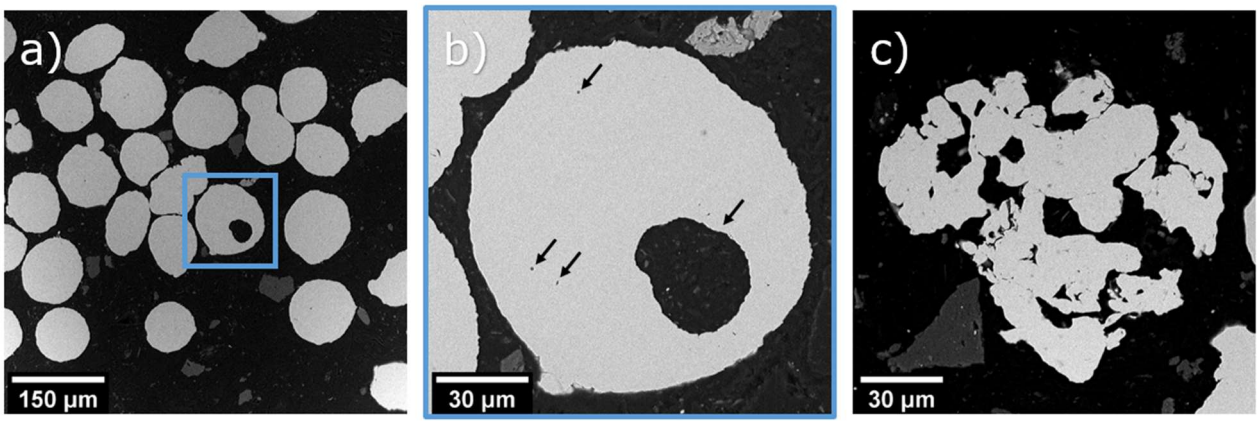

Figure 6. Cross-section SEM images of (a, b) AISI 316L and (c) Cu MP.

Figure 7 shows the density on the cross-section of PTA-deposited material. For all powder mixtures, the mean density measured were at least 99.90 %, which can be considered a good density. Although, some porosity was observed in the particles of AISI 316L powder, the as deposited stainless-steel did not show big porosities. The presence of Cu MPs had a positive impact on part density, rising it to a mean value of 99.93 %. Showing that the irregularities of Cu MPs was not a problem for PTA processing. For the nanocomposite powders of Cu NPs and Cu O NPs, no impact of the mean density was observed.

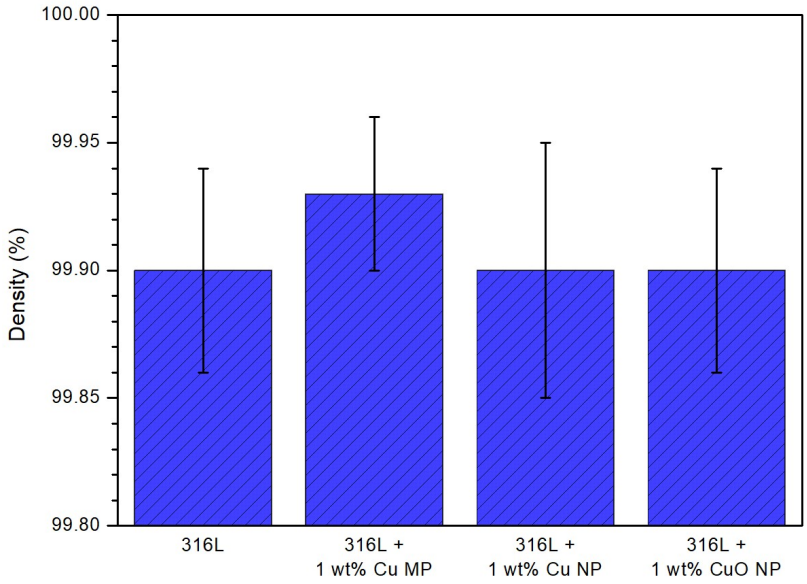

Figure 7. Density of the PTA-deposited material.

To evaluate if the nanoparticles were successfully delivered to the melt pool and consequently to the solid part, XRF of the PTA-deposited material was performed. Table 2 displays the chemical composition of the PTA-deposited materials. It is expected some variation between the powder mixture and the deposited material since the deposition process brings elements from the substrate material (AISI 304L) due to dilution. Since AISI 304L does not have Mo in its composition, a reduction in Mo percentage is observed for all powder mixtures. The addition of Cu MPs successfully increased Cu content on the solid part, about 0.94 wt%, slightly shorter than the 1.0 wt% in the powder mixture. Which again, can be explained by the dilution with the substrate material, that does not have Cu in its composition. This result shows that, the mixture between two MPs within the same size distribution range, guarantee the chemical composition of the final part.

For both nanocomposite powder, the chemical composition in the PTA-deposited material falls short on Cu content. For Cu NP and CuO NP nanocomposite powders, the difference on Cu content was 0.27 wt% and 0.10 wt%, respectively. Parts of the NPs could have remained unstable in carrier particle surface, thus parts of it segregated during powder handling and processing. In addition, a partial vaporization of the NPs in the plasma arc is expected to occur, as stated in (Prass and d'Oliveira, 2023).

Table 2. Chemical composition of the PTA-deposited material in weight percentage.

Material	Fe	Cr	Ni	Mo	Mn	S	Si	P	Cu	O
AISI 316L	Bal.	17.41	12.38	2.56	1.57	1.05	0.74	-	-	-
AISI 316L + Cu MP	Bal.	17.30	12.29	2.56	1.53	1.03	0.50	-	0.94	-
AISI 316L + Cu NP	Bal.	17.35	12.41	2.59	1.55	1.03	0.56	-	0.73	-
AISI 316L + CuO NP	Bal.	17.26	12.39	2.58	1.38	1.03	0.55	0.08	0.70	*

*Oxygen was not quantified and carbon content < 0.03 wt. %.

4. CONCLUSIONS

In this study, the preparation and characterization of nanocomposite powders for additive manufacturing (AM) were investigated. By incorporating Cu microparticles, Cu nanoparticles and CuO nanoparticles into AISI 316L powder, advanced materials with tailored properties can be further developed, opening new opportunities for applications in AM. the major conclusions from the tested conditions are as follows:

- Addition of different Cu particles had minimal impact on the elemental percentage of AISI 316L, enabling customized powder compositions without significantly altering the stainless-steel chemical composition.
- Powder mixture of AISI 316L with 1 wt% Cu MP and nanocomposite powders of AISI 316L with 1 wt% Cu NP and 1 wt% CuO NP were successfully prepared and deposited using plasma transferred arc, resulting in high-density parts (over 99.90 %).
- Morphological analyses showed distinct shape between AISI 316L particles and Cu MP. However, the powder mixture exhibited uniformly distributed Cu particles, facilitated by the powder size distributions, that were in the same range.
- For the nanocomposite powders, successful adhesion of Cu NP and CuO NP onto the carrier particle surface was achieved. The stainless-steel particle surface was partially covered by Cu NP and completely covered by CuO NP due to their different sizes.
- The presence of Cu MP and Cu NP had no impact on powder flow time. While the addition of CuO NPs increased cohesion forces between the carrier particles, increasing flow time.
- Cu content on the PTA-deposited parts remained consistent with the powder mixture containing Cu MPs. However, parts deposited with both nanocomposite powders fall short in Cu content. Requiring specific procedures to mix, handle and process these special powders.

5. ACKNOWLEDGEMENTS

The authors would like to thank LAMSE and LATECME for providing the equipment used in some of the analyses.

6. REFERENCES

Abu-Lebdeh, T. M., Damptey, R., Ungureanu, L. M., Petrescu, F. I. T., 2022, A Ternary Model for Particle Packing Optimization, Journal of Composites Science, Vol. 6, pp. 113.

American Society for Testing and Materials, 2020, ASTM B213-20: Standard Test Methods for Flow Rate of Metal Powders Using the Hall Flowmeter Funnel".

American Society for Testing and Materials, 2020, ASTM B822-20: Standard Test Method for Particle Size Distribution of Metal Powders and Related Compounds by Light Scattering".

Avrampos, P., Vosniakos, G.-C., 2022, A review of powder deposition in additive manufacturing by powder bed fusion, Journal of Manufacturing Processes, Vol. 74, pp. 332–352.

Cui, C., Becker, L., Gärtner, E., Boes, J., Lentz, J., Uhlenwinkel, V., Steinbacher, M., Weber, S., Fechte-Heinen, R., 2022, Laser Additive Manufacturing of Duplex Stainless Steel via Powder Mixture, Journal of Manufacturing and Materials Processing, Vol. 6, pp. 72.

Dong, Y., Li, Y., Ebel, T., Yan, M., 2020, Cost-affordable, high-performance Ti–TiB composite for selective laser melting additive manufacturing, Journal of Materials Research, Vol. 35, pp. 1922–1935.

Garg, R., Dhami, H. S., Panda, P. R., Viswanathan, K., 2023, Evaluating gas-driven flow mechanics of non-spherical powders for directed energy deposition, Journal of Manufacturing Processes, Vol. 99, pp. 260–271.

Huang, Y., Leu, M. C., Mazumder, J., Donmez, A., 2015, Additive Manufacturing: Current State, Future Potential, Gaps and Needs, and Recommendations, Journal of Manufacturing Science and Engineering, Vol. 137.

Li, N., Huang, S., Zhang, G., Qin, R., Liu, W., Xiong, H., Shi, G., Blackburn, J., 2019, Progress in additive manufacturing on new materials: A review, Journal of Materials Science & Technology, Vol. 35, pp. 242–269.

Mellin, P., Lyckfeldt, O., Harlin, P., Brodin, H., Blom, H., Strondl, A., 2017, Evaluating flowability of additive manufacturing powders, using the Gustavsson flow meter, Metal Powder Report, Vol. 72, pp. 322–326.

Prass, G. S., d'Oliveira, A. S. C. M., 2023, Processing and characterization of AISI 316L coatings modified with Cu and CuO nanoparticles, Surface and Coatings Technology, Vol. 461, pp. 129465.

Sharma, R., Setia, G., 2019, Mechanical dry particle coating on cohesive pharmaceutical powders for improving flowability - A review, Powder Technology, Vol. 356, pp. 458–479.

Soulier, M., Benayad, A., Teulon, L., Oudart, Y., Senol, S., Vanmeensel, K., 2022, Nanocomposite powder for powder-bed-based additive manufacturing obtained by dry particle coating, Powder Technology, Vol. 404, pp. 117474.

Zhuang, J., Gu, D., Xi, L., Lin, K., Fang, Y., Wang, R., 2020, Preparation method and underlying mechanism of MWCNTs/Ti6Al4V nanocomposite powder for selective laser melting additive manufacturing, Powder Technology, Vol. 368, pp. 59–69.

7. RESPONSIBILITY NOTICE

The authors are the only responsible for the printed material included in this paper.